Experimental Evaluation of Nonlinear Feedback and Feedforward Control Schemes for Manipulators

Pradeep K. Khosla and Takeo Kanade

CMU-RI-TR-87-4

Department of Electrical and Computer Engineering
The Robotics Institute
Carnegie Mellon University
Pittsburgh, Pennsylvania 15213

March 1987

This research is based upon the work supported by the National Science Foundation under Grant ECS-8320364.

Table of Contents

Abstract

The manipulator trajectory tracking control problem revolves around computing the torques to be applied to achieve accurate tracking. While this problem has been extensively studied in simulations, the real-time results have been lacking in the robotics literature. In this paper, we present the experimental results of the real-time performance of model-based control algorithms. We compare the computed-torque control scheme with the feedforward dynamics compensation scheme. The feedforward scheme compensates for the manipulator dynamics in the feedforward path while the computed-torque scheme uses the dynamics in the feedback loop for linearization and decoupling. The manipulator control schemes have been implemented on the CMU DD Arm II with a sampling period of 2 ms.

1. Introduction

The manipulator control problem revolves around the computation of the joint torques required to track the desired joint position, velocity and acceleration trajectories. This problem has been studied extensively in the robotics literature and many schemes have been proposed [3, 4, 5, 6, 14, 15]. While many simulation results have been presented, the real-time implementation and performance evaluation of model-based control schemes on actual manipulators has not been performed. The main reasons for this are: (1) the high gear ratios and the dominant friction effects in commercial geared manipulators make them unsuitable for real-time performance evaluation; (2) the computational requirements of the Newton-Euler algorithm are still beyond the reach of commercially available microprocessors [7] for high sample-rate control; and (3) it has been difficult to obtain an accurate model because research in this area has been lacking.

One of the goals of the CMU Direct-Drive Arm II [13] project is to demonstrate the effect of full dynamics compensation on the real-time trajectory performance tracking of manipulators by overcoming the above mentioned difficulties. To overcome the hurdle posed by the computational requirements, we have customized the Newton-Euler algorithm and achieved a computational cycle of 1.2 ms. This permits us to implement control algorithms at high sampling rates of up to 830 Hz. We have also proposed numerical [8] and symbolic algorithms [9, 12] to estimate the dynamics parameters of a manipulator. We have implemented our algorithm on the CMU Direct-Drive Arm II to obtain an accurate dynamics model.

The above developments have allowed us the opportunity to implement and evaluate the real-time performance of advanced manipulator control schemes. The experimental results of the real-time implementation and evaluation of model-based control schemes were presented recently, wherein the performance of the computed-torque and the independent joint control schemes was compared [10]. Other researchers have also investigated this problem and evaluated the real-time performance of the model-based schemes [11, 1].

In this paper, we compare the computed-torque scheme with the feedforward dynamics compensation scheme. Both the schemes use the full dynamics model of the manipulator but in different paths of the control loop: the feedforward scheme compensates for the manipulator dynamics in the feedforward path while the computed-torque scheme uses the dynamics in the feedback loop for linearization and decoupling. The control schemes have been implemented on the CMU DD Arm II with a sampling period of 2 ms.

This paper is organized as follows: the manipulator control schemes that have been implemented and evaluated are presented in Section 2. The design of the controller gain matrices is outlined in Section 3. In Section 4, we delineate and analyze the results of our real-time implementation. And finally, in Section 5, we draw our conclusions.

2. Manipulator Control Techniques

The dynamics of a manipulator are described by a set of highly nonlinear and coupled differential equations. The complete dynamic model of an N degrees-of-freedom manipulator is described by:

$$\tau = \mathbf{D}(\theta)\ddot{\theta} + \mathbf{h}(\theta,\dot{\theta}) + \mathbf{g}(\theta) \tag{1}$$

where τ is the N vector of the actuating torques; $\mathbf{D}(\theta)$ is the $N \times N$ position dependent manipulator inertia matrix; $\mathbf{h}(\theta,\dot{\theta})$ is the N vector of Coriolis and centrifugal torques; $\mathbf{g}(\theta)$ is the N vector of gravitational torques; and $\ddot{\theta}$, $\dot{\theta}$ and θ are N vectors of the joint accelerations, velocities and positions, respectively.

We have implemented and compared the performance of the computed-torque and the feedforward compensation control schemes. In order to evaluate the effect of approximating the position dependent inertia matrix $\mathbf{D}(\theta)$ by a constant diagonal inertia matrix $\mathbf{J}$, we have also implemented the reduced feedforward compensation scheme. In the sequel, $\mathbf{K}_p$ and $\mathbf{K}_v$ are the constant and diagonal position and velocity feedback gain matrices, repectively; θ and θ_d are the measured and the reference joint position vectors, repectively; and the symbol "." denotes the derivative with respect to time.

Computed-Torque Control Scheme (CT)

This scheme, depicted in Figure 1, utilizes nonlinear feedback to decouple the manipulator. The control torque τ is computed by the inverse dynamics equation in (1), using the commanded acceleration instead of the measured acceleration $\ddot{\theta}$, as:

$$\tau = \tilde{\mathbf{D}}(\theta)[\mathbf{K}_p(\theta_d - \theta) + \mathbf{K}_v(\dot{\theta}_d - \dot{\theta}) + \ddot{\theta}_d] + \tilde{\mathbf{h}}(\theta,\dot{\theta}) + \tilde{\mathbf{g}}(\theta) \tag{2}$$

where the "~" indicates that the estimated values of the dynamics parameters are used in the computation.

Feedforward Dynamics Compensation Scheme (FED)

If the dynamics model of a manipulator is *exact*, then the application of joint torques computed from equation (1) by using the reference trajectory will accomplish trajectory tracking. In practice, however, the presence of modeling errors creates the need for a feedback controller to compensate for the small deviations in trajectory tracking. The feedforward dynamics compensation technique, depicted in Figure 2, is based on the premise that the gross torque for trajectory tracking is provided by using the inverse dynamics model in equation (1) in the feedforward path. This control signal is then augmented with the signal derived from linear independent joint controllers which are assumed to correct for small deviations in trajectory tracking. The control torque τ is therefore:

$$\tau = \tilde{\mathbf{D}}(\theta_d)\ddot{\theta}_d + \tilde{\mathbf{h}}(\theta_d,\dot{\theta}_d) + \tilde{\mathbf{g}}(\theta_d) \\ + \mathbf{J}[\mathbf{K}_p(\theta_d-\theta) + \mathbf{K}_v(\dot{\theta}_d-\dot{\theta})] \tag{3}$$

where the first three terms are the feedforward compensation torque, the last term is the torque due to the feedback controller, and **J** is the $N\times N$ diagonal matrix of link inertias at a typical position.

Reduced Feedforward Compensation Scheme (RFED)

The reduced feedforward compensation scheme, depicted in Figure 3, has been implemented to demonstrate the effect of approximating the position dependent inertia matrix by a constant diagonal matrix. The control torque is computed by substituting the constant diagonal inertia matrix **J** instead of $\mathbf{D}(\theta_d)$ in the first term in equation (3). Thus the torque applied to the joints at each sampling instant is:

$$\tau = \mathbf{J}[\mathbf{K}_p(\theta_d-\theta) + \mathbf{K}_v(\dot{\theta}_d-\dot{\theta}) + \ddot{\theta}_d] \\ + \tilde{\mathbf{h}}(\theta_d,\dot{\theta}_d) + \tilde{\mathbf{g}}(\theta_d) \tag{4}$$

where τ is the N vector of applied control torques and **J** is the $N\times N$ diagonal matrix of link inertias at a typical position.

The application of the above control laws is based on the assumption that the joint drive system is a torque controlled device. To ensure that the above assumption is satisfied, we have identified the characteristics of the joint drive systems. The CMU DD Arm II has very little friction, and is driven by brushless DC-torque motors with the amplifiers which control motor current rather than voltage or speed.

We conducted the open-loop small-signal frequency response analysis and identified the continuous-time transfer function of each joint. Since our sampling period of 2 *ms* is about 10 times smaller than the dominant mechanical time constant of the system, we assume that the effects of sampling are not evident in the input-output response of the system: this assumption is indeed supported by the results of the experiment. The identified transfer functions are depicted in Table 1.

3. Controller Design

The performance of the control schemes presented in the previous section can be compared only if the same criteria are used for design of the controller gain matrices. Fortunately, this is possible because the gain matrices $\mathbf{K}_p$ and $\mathbf{K}_v$ are the same for all the three control schemes presented in this paper. The detailed procedure for choosing these

gain matrices and establishing an equivalence between the gains of the nonlinear computed-torque scheme and the linear independent joint control scheme is outlined by Khosla and Kanade [10]. For expository convenience, we outline the criteria for the selection of the gain matrices for the computed-torque scheme. In our experiments, we used these gain values for implementing and evaluating the performance of the RFED and FED schemes also.

3.1. Design of Gain Matrices for Computed-Torque Scheme

The basic idea behind the computed-torque scheme is to achieve dynamic decoupling of all the joints using nonlinear feedback. If the dynamic model of the manipulator is described by equation (1) and the applied control torque is computed according to equation (2), then the following closed-loop system is obtained [15]:

$$\ddot{\theta} = \mathbf{u}_i - [\tilde{\mathbf{D}}]^{-1}\{[\mathbf{D} - \tilde{\mathbf{D}}]\ddot{\theta} + [\mathbf{h} - \tilde{\mathbf{h}}] + [\mathbf{g} - \tilde{\mathbf{g}}]\}$$

where $\mathbf{u}_i$ is the commanded acceleration signal and the functional dependencies on θ and $\dot{\theta}$ have been omitted for the sake of clarity. If the dynamics are modeled exactly, that is, $\tilde{\mathbf{D}}$=$\mathbf{D}$, $\tilde{\mathbf{h}}$=$\mathbf{h}$ and $\tilde{\mathbf{g}}$=$\mathbf{g}$, then the decoupled closed loop system is described by

$$\ddot{\theta} = \mathbf{u}_i. \tag{5}$$

The commanded acceleration signal [10] is typically computed as:

$$\mathbf{u}_i = \mathbf{K}_p(\theta_d - \theta) + \mathbf{K}_v(\dot{\theta}_d - \dot{\theta}) + \ddot{\theta}_d \tag{6}$$

and its substitution in equation (5) results in the following closed-loop characteristic equation for all the joints:

$$s^2 + k_{vj}s + k_{pj} = 0 \tag{7}$$

where k_{vj} and k_{pj} are the velocity and position gains for the *j-th* joint.

Since it is desired that none of the joints overshoot the commanded position or the response be critically damped, our choice of the matrices $\mathbf{K}_p$ and $\mathbf{K}_v$ must be such that their elements satisfy the condition:

$$k_{vj} = 2\sqrt{k_{pj}} \qquad \text{for j} = 1,.....,6 \tag{8}$$

Besides, in order to achieve a high disturbance rejection ratio or high stiffness, it is also necessary to choose the position gain matrix $\mathbf{K}_p$ as large as possible, which results in a large $\mathbf{K}_v$.

In practice, however, the choice of the velocity gain $\mathbf{K}_v$ is limited by the noise present in the velocity measurement. We determined the upper limit of the velocity gain

experimentally: we set the position gain to zero and increased the velocity gain of each joint until the unmodeled high-frequency dynamics of the system were excited by the noise introduced in the velocity measurement. This value of K_v represents the maximum allowable velocity gain. We chose 80% of the maximum velocity gain in order to obtain as high value of the position gain as possible and still be well within the stability limits with respect to the unmodeled high frequency dynamics. The elements of the position gain matrix K_p were computed to satisfy the critical damping condition in equation (8) and achieved the maximum disturbance rejection ratio, also. The elements of the velocity and position gain matrices used in the implementation of the control schemes are listed in Table 1.

4. Experiments and Results

4.1. Trajectory Selection and Evaluation Criteria

Since the DD Arm II is a highly nonlinear and coupled system it is impossible to characterize its behavior from a particular class of inputs, unlike linear systems for which a specific input (such as a unit step or a ramp) can be used to design and evaluate the controllers. Thus an important constituent of the experimental evaluation of robot control schemes is the choice of a class of inputs for the robot. The criteria for selecting the joint trajectories is detailed by Khosla [8].

For evaluating the performance of robot control schemes, we use the dynamic tracking accuracy. This is defined as the maximum position and velocity tracking error along a specified trajectory.

4.2. Real-Time Results

We have implemented the control schemes CT, FED and RFED, presented in Section 2, and evaluated their real-time performance on the six degrees-of-freedom CMU DD Arm II. Because of lack of space, we present our results for a simple but illustrative trajectory used to evaluate the above mentioned control schemes.

The trajectory is chosen to be simple and relatively slow, but capable of providing insight into the effect of dynamics compensation. In this trajectory, only joints 1 and 2 move while all the other joints are commanded to hold their zero positions and can be envisioned from the schematic diagram in Figure 4. Joint 1 is commanded to start from its zero position and to reach the position of 1.5 rad in 0.75 seconds; it remains at this position for an interval of 0.75 seconds after which it is required to return to its home position in 0.75 seconds. Similarly, joint 2 is commanded to start from its zero position and to reach the position of -1.5 rad in 0.75 seconds; it remains at this position for an interval of 0.75 seconds after which it is required to return to its home position in 0.75 seconds. The points of discontinuity, in the trajectory, were joined by a fifth-order polynomial to maintain the

continuity of position, velocity and acceleration along the three segments. The desired position, velocity and acceleration trajectories for joints 1 and 2 are depicted in Figures 5 and 6, respectively. The absolute value of the maximum velocity and acceleration to be attained by joints 1 and 2 are 2 rad/sec and 7.5 rad/sec^2, respectively.

The position and velocity tracking curves for the schemes CT, RFED and FED are depicted in Figures 7 through 10. The corresponding position and velocity tracking errors in the three schemes for each joint are shown in Figures 11 through 16. To give an idea of the relative performances, the maximum position and velocity tracking errors of each joint are depicted in Table 2. For the sake of brevity we have not included the graphs or tabulated the values of the errors of the last three wrist joints.

To provide us with insight and to aid in the interpretation of the results, we outline the dynamic equations for the first three degrees-of-freedom of the CMU DD Arm II:

$$\tau_1 = d_{11}\ddot{\theta}_1 + d_{12}\ddot{\theta}_2 + d_{13}\ddot{\theta}_3 + h_{133}\dot{\theta}^2_3 + h_{122}\dot{\theta}^2_2 + 2h_{123}\dot{\theta}_2\dot{\theta}_3 + 2h_{113}\dot{\theta}_1\dot{\theta}_3 + 2h_{112}\dot{\theta}_1\dot{\theta}_2 \tag{9}$$

$$\tau_2 = d_{21}\ddot{\theta}_1 + d_{22}\ddot{\theta}_2 + d_{23}\ddot{\theta}_3 + h_{233}\dot{\theta}^2_3 + h_{223}\dot{\theta}_2\dot{\theta}_3 + 2h_{213}\dot{\theta}_1\dot{\theta}_3 - h_{211}\dot{\theta}^2_1 \tag{10}$$

$$\tau_3 = d_{31}\ddot{\theta}_1 + d_{32}\ddot{\theta}_2 + d_{33}\ddot{\theta}_3 - h_{322}\dot{\theta}^2_2 - 2h_{312}\dot{\theta}_1\dot{\theta}_2 - h_{311}\dot{\theta}^2_1 + g_3 \tag{11}$$

The coefficients d_{ij}, h_{ijk} and g_i are functions of the joint position vector θ and are detailed by Khosla and Kanade [9].

The applied torque signals for the three schemes are shown in Figures 17–19. Further, decomposition of the applied torques in CT into the inertial, the centrifugal and Coriolis, and the gravity components of joints 1 through 3 is presented in Figures 20–22. We note that the applied torque for joint 1 has a profile similar to the desired acceleration of joint 1 except during the periods of constant speed (0.75 to 1.0 sec and 2.25 to 2.5 sec) in the trajectory. This suggests that the inertial torque $d_{11}\ddot{\theta}_1$ dominates along most part of the trajectory. This is further supported by the profile of the inertial torque component in Figure 20. The deviations observed in Figure 20 are due to the Coriolis and the centrifugal components of the applied torque which dominate during the period of constant velocity.

In the case of joint 2, the inertial component of the applied torque curve in Figure 21 is similar to the profile of the desired acceleration of joint 1 in Figure 5. This implies that the

applied torque of joint 2 is dominated by the inertial coupling term $d_{21}\ddot{\theta}_1$ along most of the trajectory. The term $h_{211}\dot{\theta}^2{}_1$ in equation (10) constitutes the centrifugal torque and is seen to dominate during periods of constant velocity.

Finally, in Figure 22 the inertial component of the applied torque of joint 3 has a profile similar to the desired acceleration of joint 2, when the velocity dependent torques are negligible. This implies that the inertial coupling term $d_{32}\ddot{\theta}_2$ dominates along most part of the trajectory. The gravitational torque in Figure 22 is due to the position errors and is negligible compared to the other torque components. It may be seen from equation (11) that the nonlinear velocity dependent torque consists of both the Coriolis and the centrifugal components arising out of the movement of links 1 and 2.

5. Conclusions

The aim of this paper has been twofold: first, to compare the performance of the feedforward dynamics compensation scheme with the computed-torque scheme, and second, to underscore the need for including the off-diagonal elements of the inertia matrix in the torque computation. The latter has been considered to be important particularly in the case of direct-drive arms where the inertial coupling effects are accentuated due to lack of gears [2]. It has been demonstrated in our experiments and further supported by our analysis that it is possible for the off-diagonal terms to completely dominate the diagonal terms of the inertial matrix in the computation of the joint actuating torques. In such an event neglecting the off-diagonal terms may lead to trajectory tracking errors. It must also be pointed out that if an *exact* model of the manipulator were available then both the computed-torque and feedforward compensation scheme will give similar results. In such a circumstance, using the feedforward dynamics compensation may have some implementational advantages because the feedforward torques could be computed off-line and added on-line to the torques computed by the independent joint controllers.

Table 1: Transfer Functions and Gains of Individual Links

Joint (j)	Transfer Function ($\frac{1}{J_j s^2}$)	k_{pj}	k_{vj}
1	$\frac{1}{12.3s^2}$	40.0	12.6
2	$\frac{1}{2s^2}$	58.0	15.2
3	$\frac{1}{0.25s^2}$	400.0	40.0
4	$\frac{1}{0.007s^2}$	2800.0	106.0
5	$\frac{1}{0.006s^2}$	1200.0	69.3
6	$\frac{1}{0.0003s^2}$	3000.0	110.0

Table 2: Maximum Tracking Errors for T1

	CT		RFED		FED	
Joint No.	Pos Error (rads)	Vel Error (rads/sec)	Pos Error (rads)	Vel Error (rads/sec)	Pos Error (rads)	Vel Error (rads/sec)
1	0.082	0.35	0.03	0.20	0.036	0.40
2	0.11	0.55	0.18	0.88	0.13	0.58
3	0.008	0.008	0.026	0.23	0.056	0.2

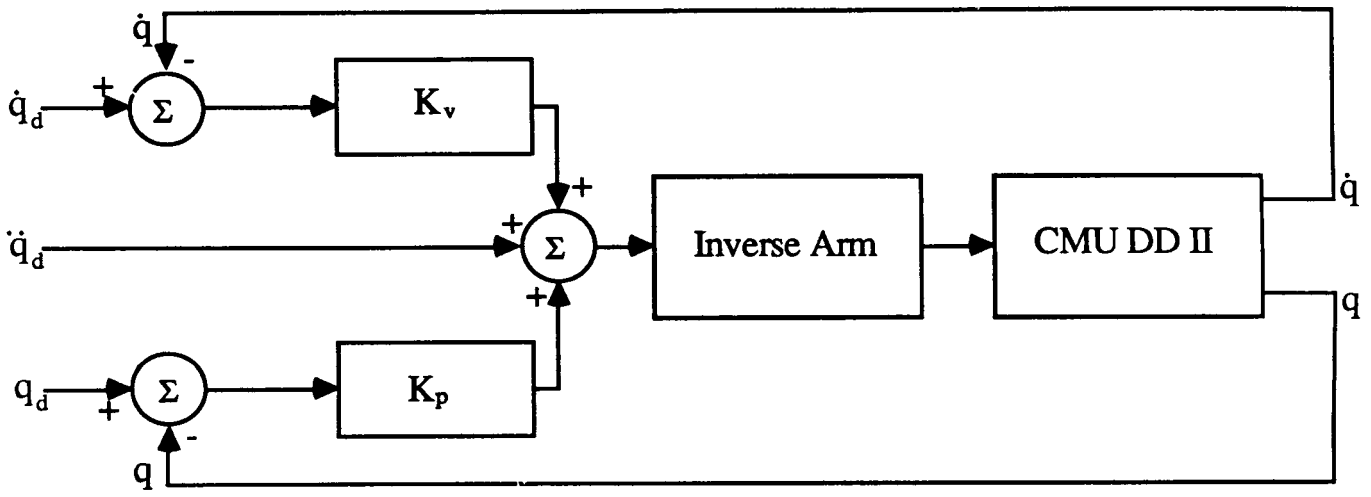

Figure 1: Block diagram of computed-torque control scheme

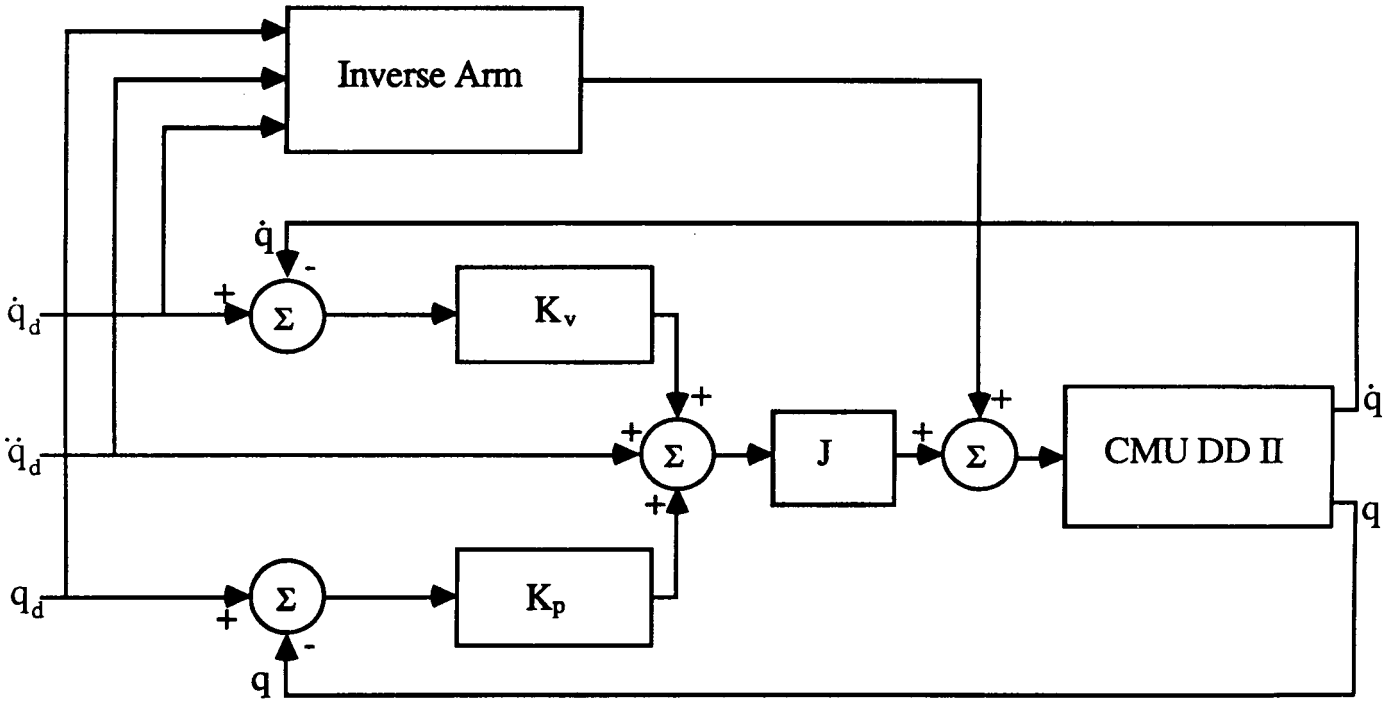

Figure 2: Block diagram of feedforward compensation control scheme

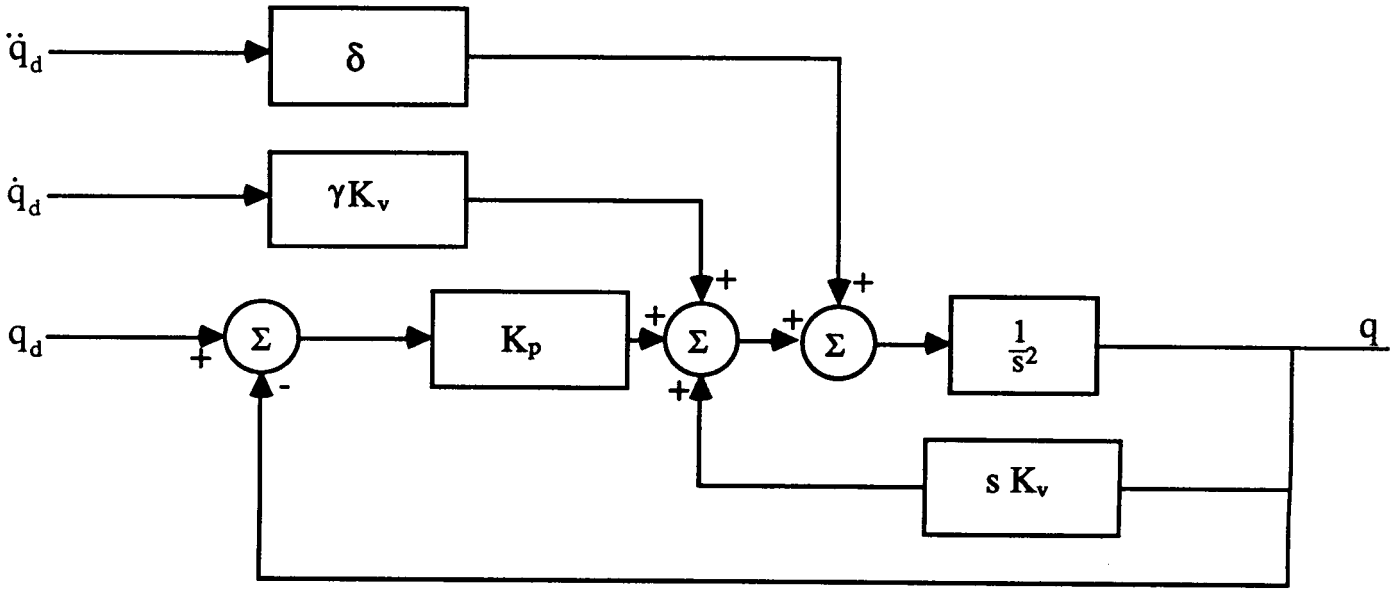

Figure 3: Block diagram of independent joint control scheme

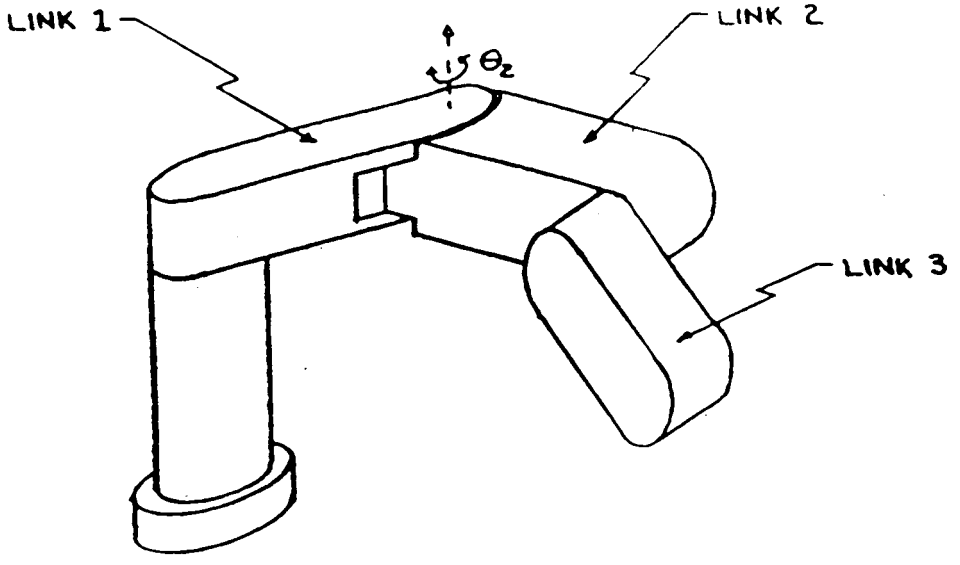

Figure 4: Schematic diagram of 3 DOF DD Arm II

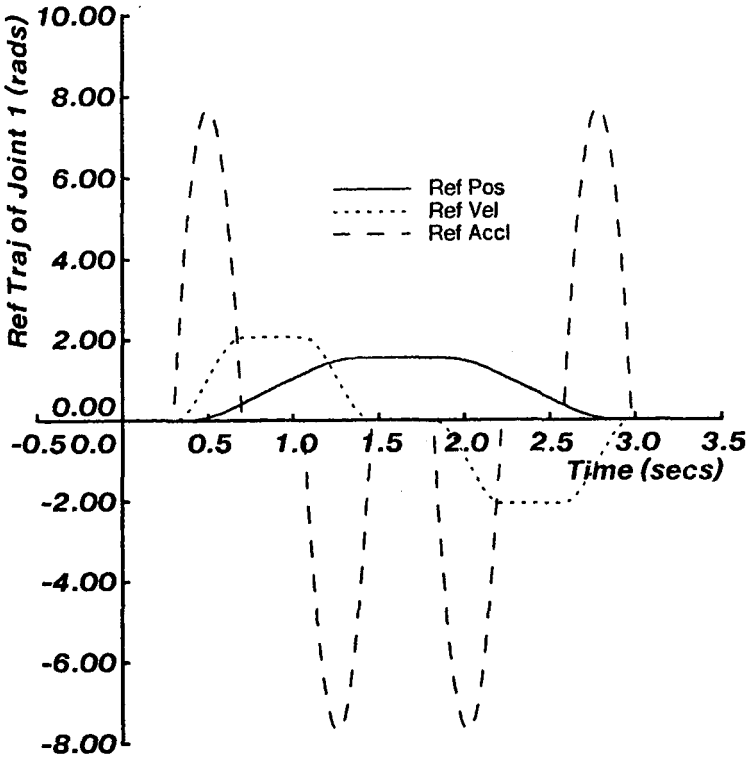

Figure 5: Desired trajectories for joint 1

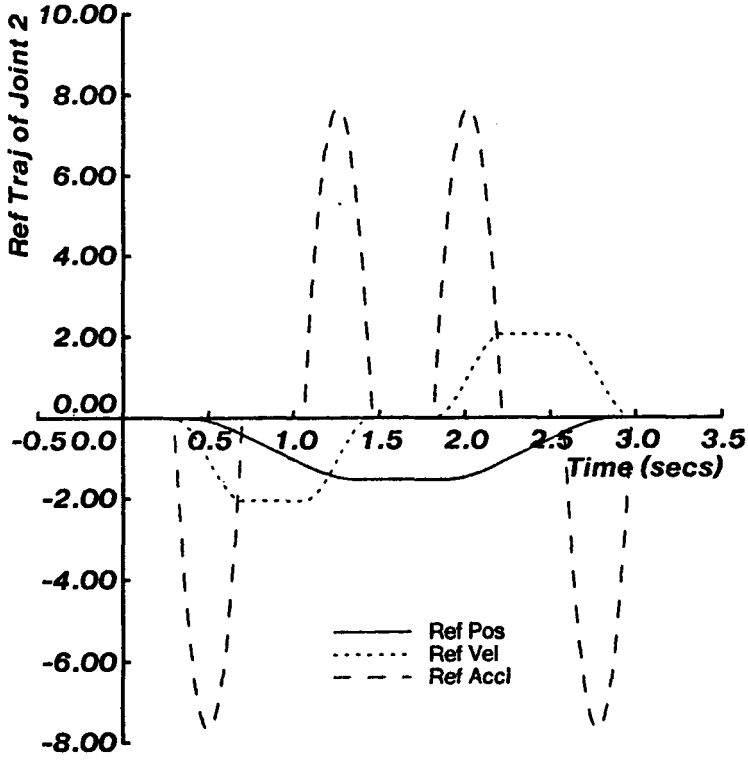

Figure 6: Desired trajectories for joint 2

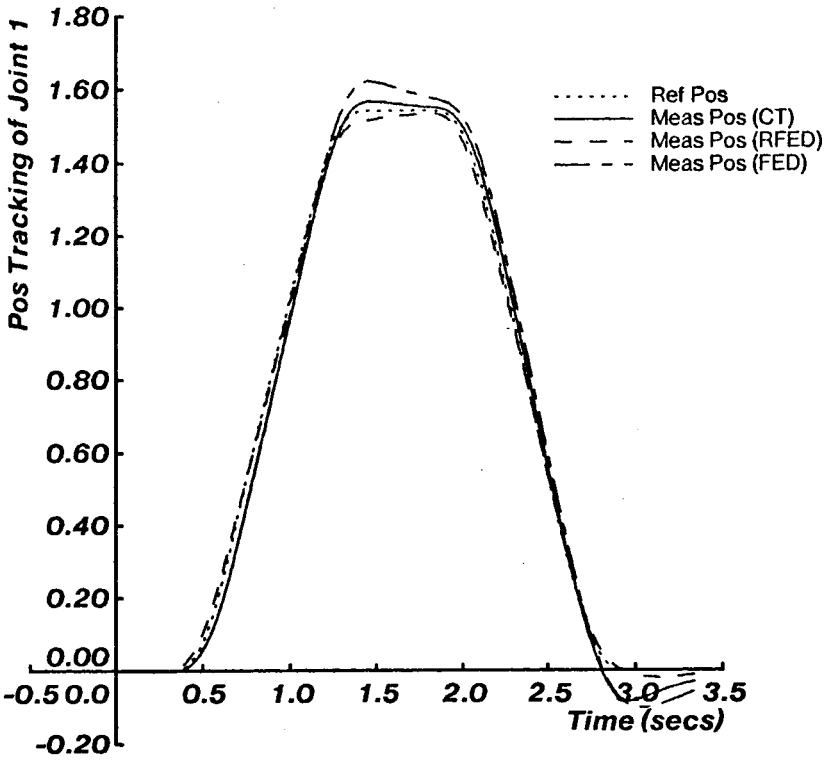

Figure 7: Position tracking of joint 1

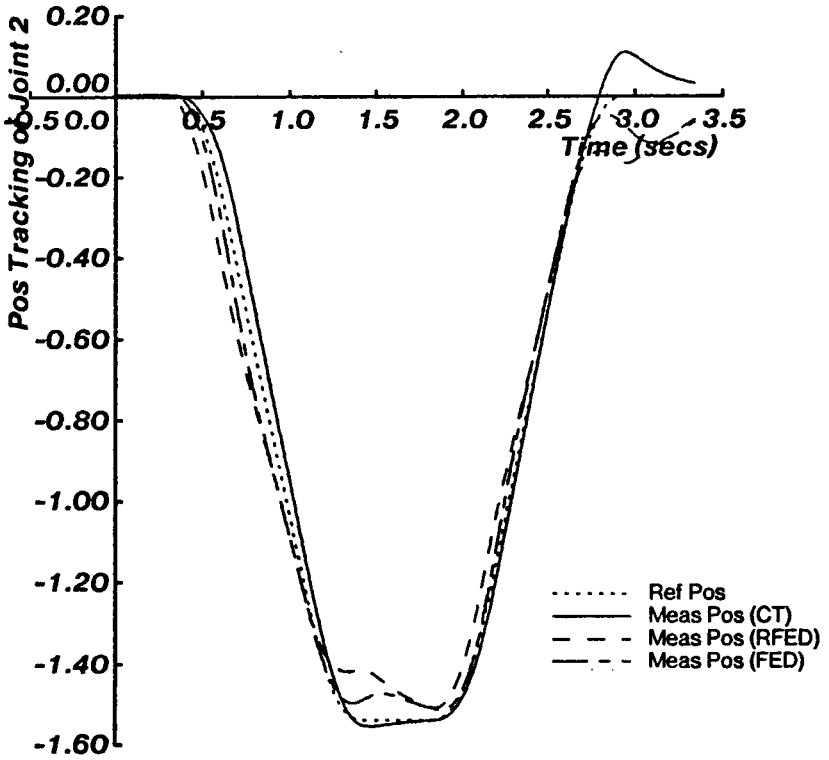

Figure 8: Position tracking of joint 2

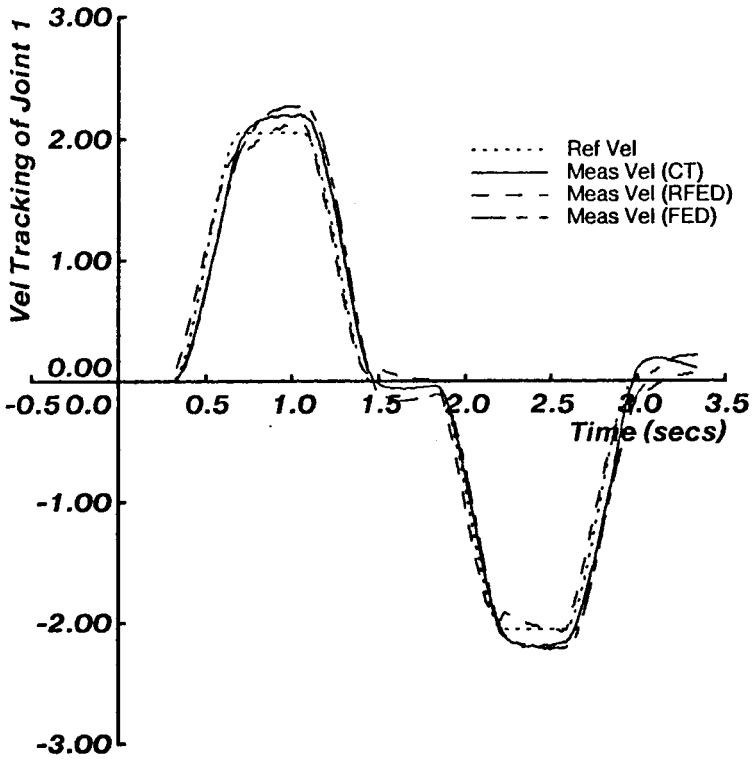

Figure 9: Velocity tracking of joint 1

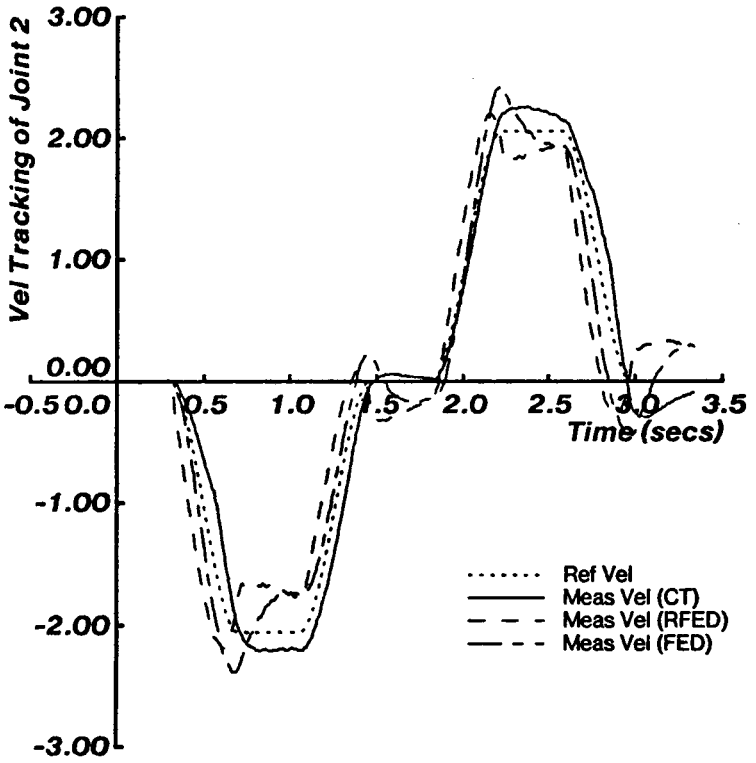

Figure 10: Velocity tracking of joint 2

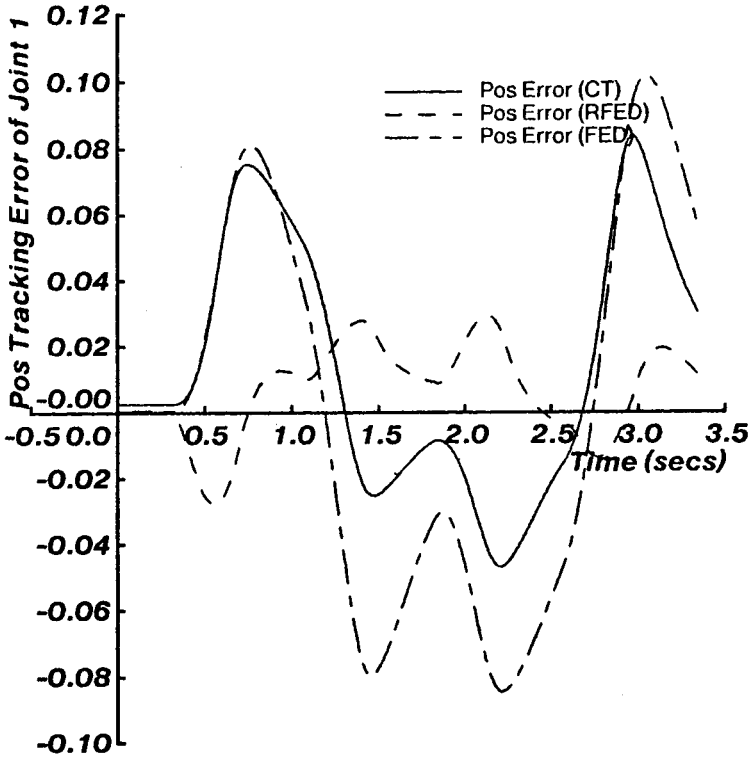

Figure 11: Position tracking errors of joint 1

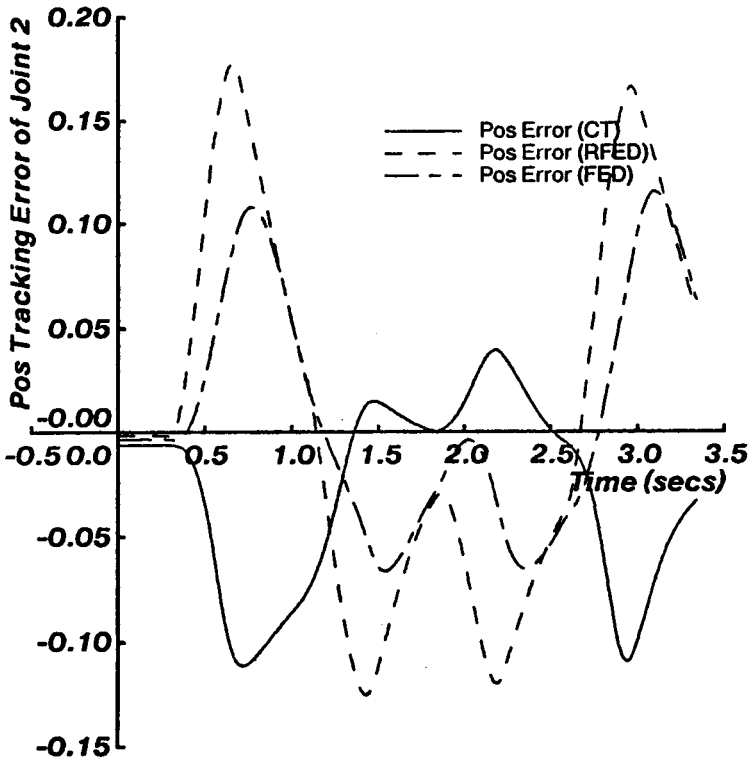

Figure 12: Position tracking errors of joint 2

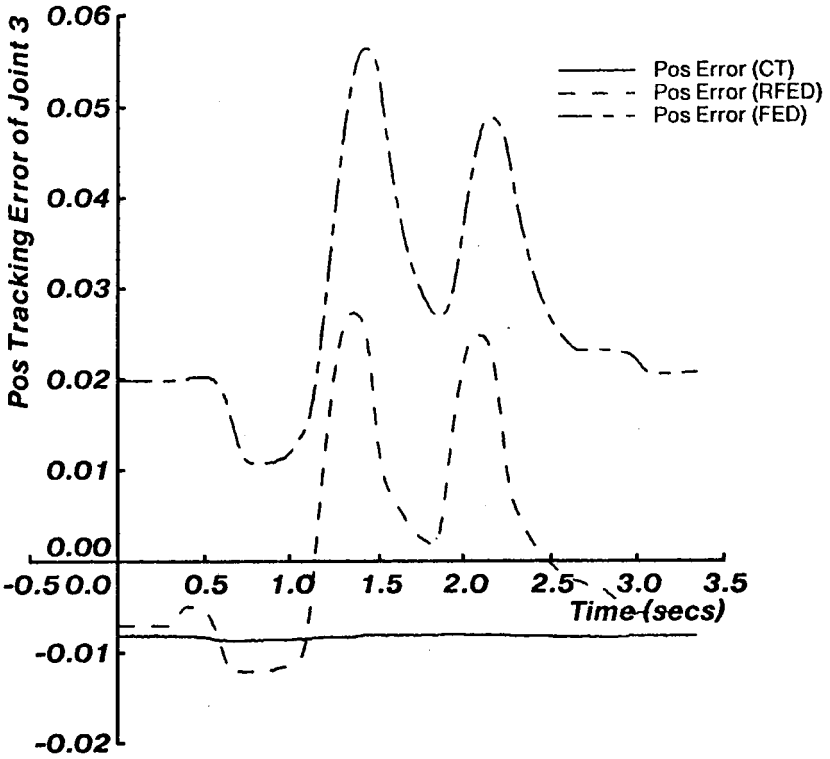

Figure 13: Position tracking errors of joint 3

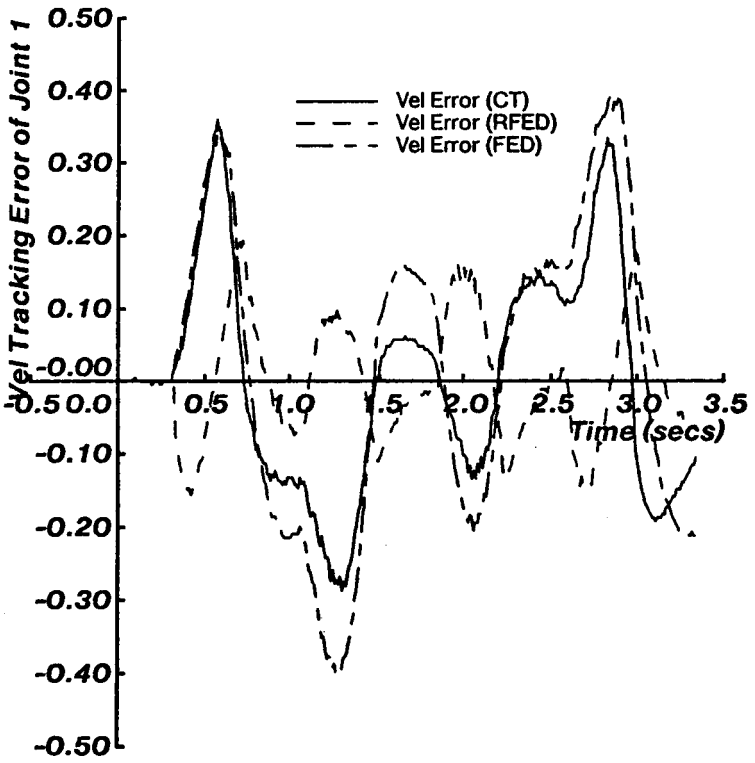

Figure 14: Velocity tracking errors of joint 1

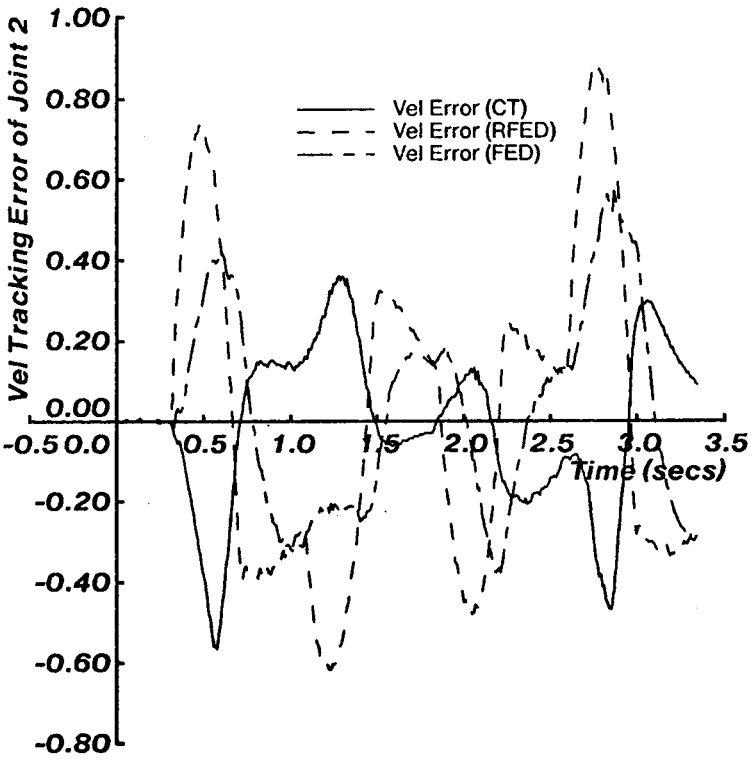

Figure 15: Velocity tracking errors of joint 2

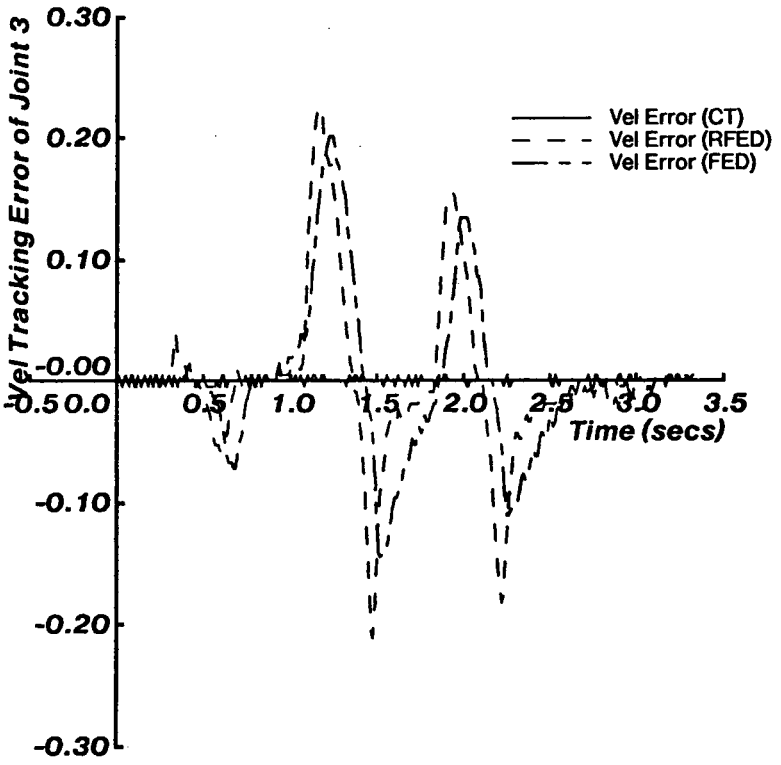

Figure 16: Velocity tracking errors of joint 3

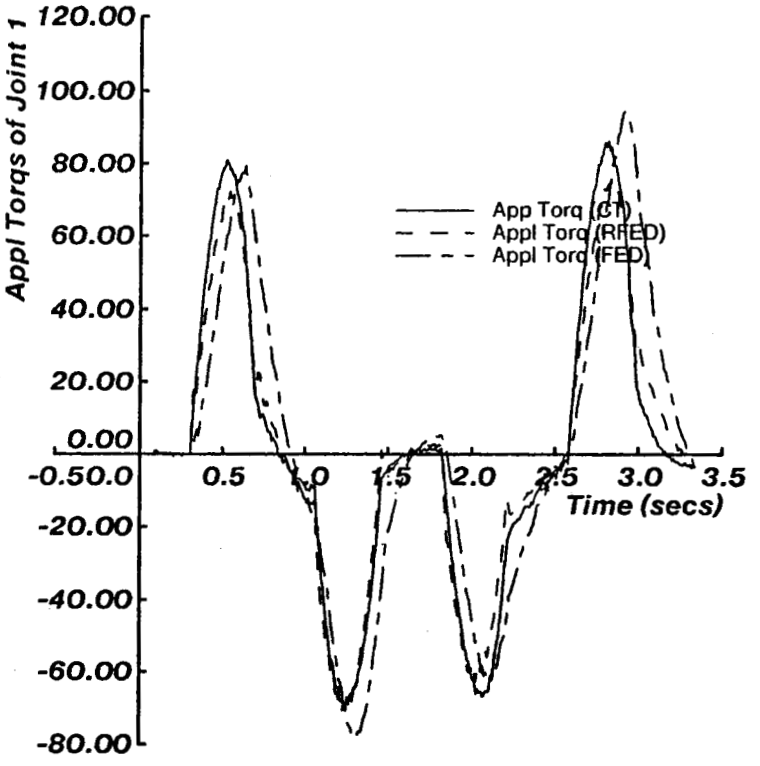

Figure 17: Applied torque of joint 1

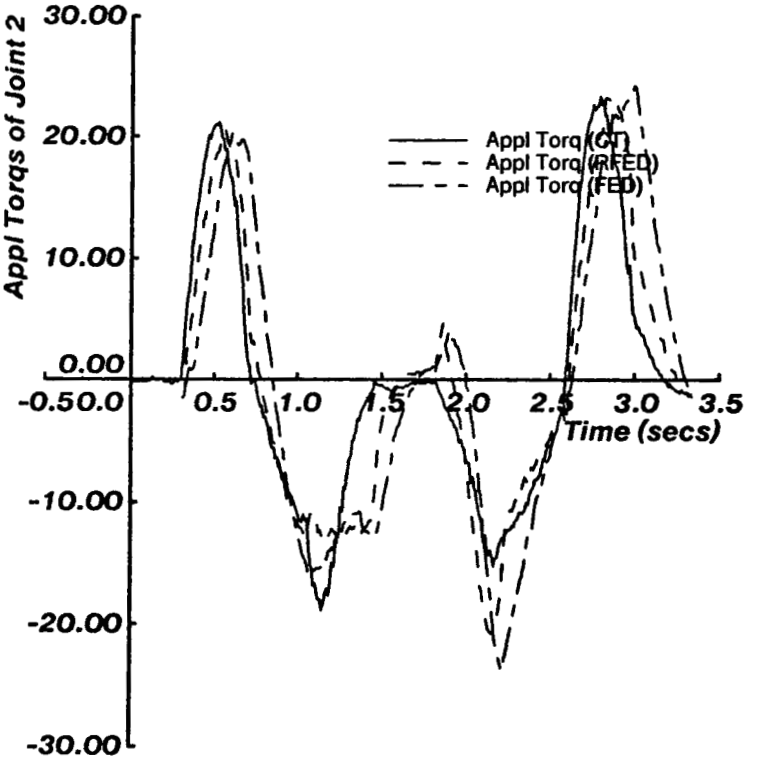

Figure 18: Applied torque of joint 2

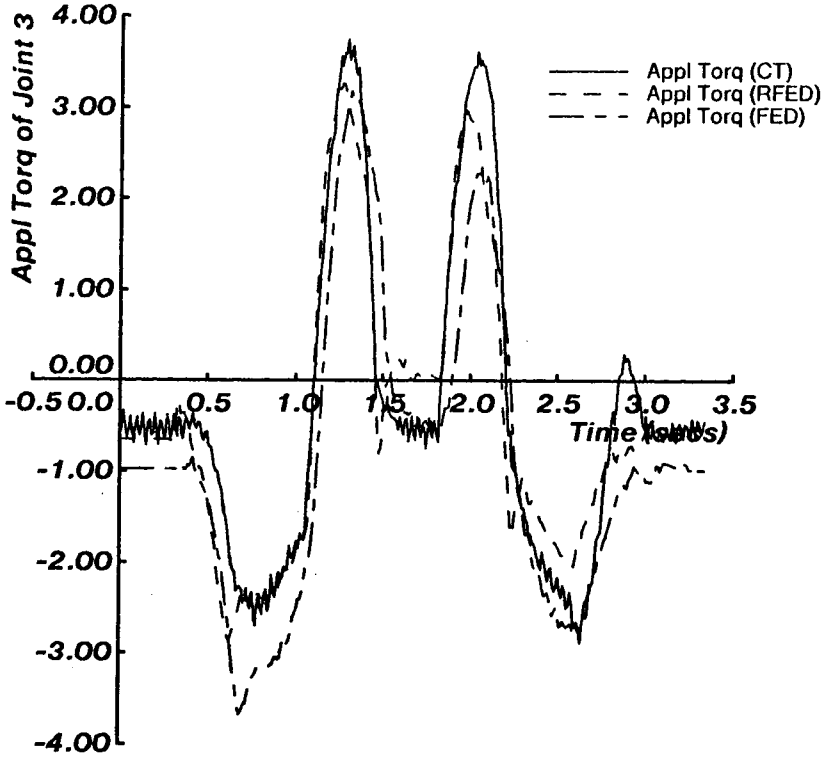

Figure 19: Applied torque of joint 3

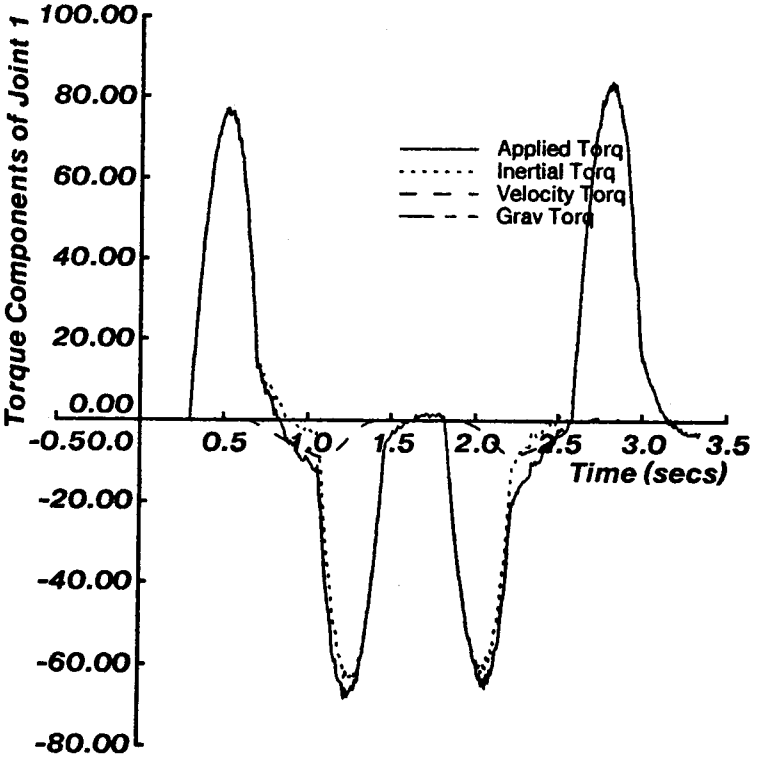

Figure 20: Torque components of joint 1 for CT

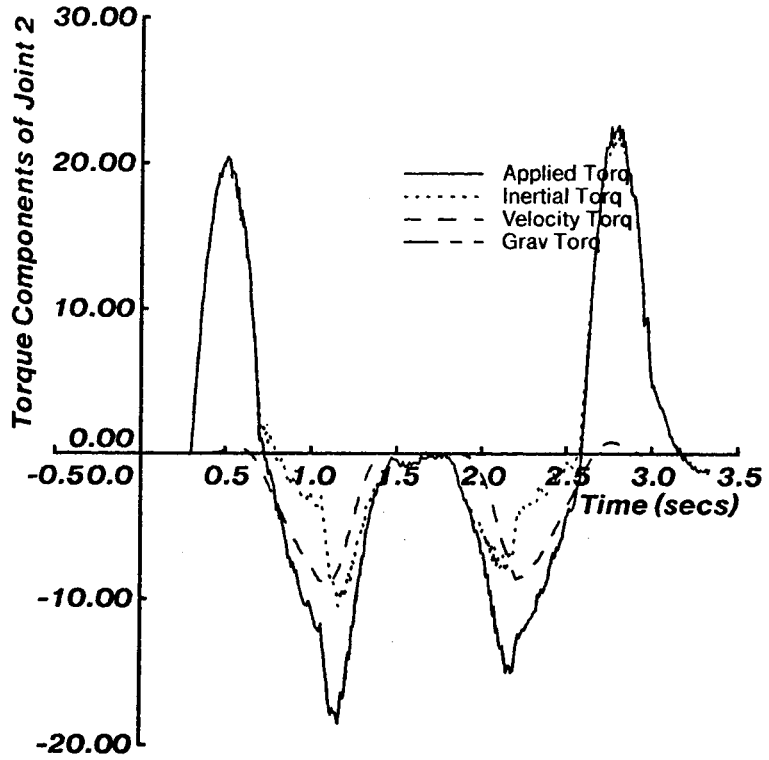

Figure 21: Torque components of joint 2 for CT

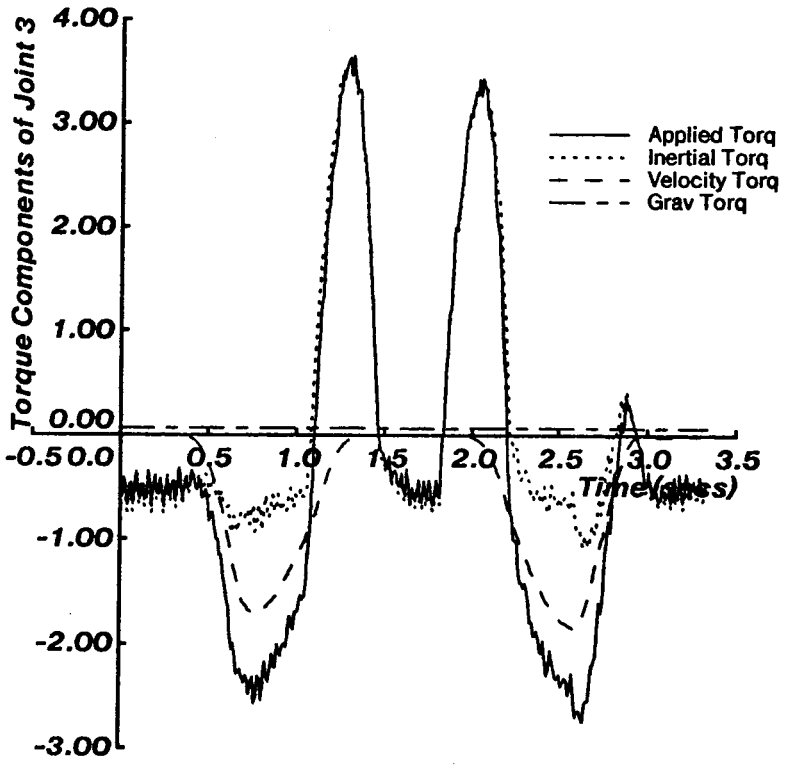

Figure 22: Torque components of joint 3 for CT

Table 3: Maximum Tracking Errors

	CT		RFED		FED	
Joint No.	Pos Error (rads)	Vel Error (rads/sec)	Pos Error (rads)	Vel Error (rads/sec)	Pos Error (rads)	Vel Error (rads/sec)
1	0.082	0.35	0.03	0.20	0.036	0.40
2	0.11	0.55	0.18	0.88	0.13	0.58
3	0.008	0.008	0.026	0.23	0.056	0.2

References

[1] An, C. H., Atkeson, C. G. and Hollerbach, J. M.
Experimental Determination of the Effect of Feedforward Control on Trajectory Tracking Errors.
In Bejczy, A. K. (editor), *Proceedings of 1986 IEEE Conference on Robotics and Automation*, pages 55-60. IEEE, San Francisco, CA, April 7-10, 1986.

[2] Asada, H., Kanade, T. and Takeyama, I.
Control of a Direct-Drive Arm.
Technical Report CMU-RI-TR-82-4, The Robotics Institute, Carnegie-Mellon University, April, 1982.

[3] Bejczy A. K.
Robot Arm Dynamics and Control.
Technical Memorandum 33-669, Jet Propulsion Laboratory, Pasadena, CA, February, 1974.

[4] Brady, M., et al. (editors).
Robot Motion: Planning and Control.
MIT Press, Cambridge, MA, 1982.

[5] Freund, E.
Fast Nonlinear Control with Arbitrary Pole Placement for Industrial Robots and Manipulators.
International Journal of Robotics Research 1(1):65-78, 1982.

[6] Horowitz, R. and Tomizuka, M.
An Adaptive Control Scheme for Mechanical Manipulators-Compensation of Nonlinearity and Decoupling Control.
In *Proceedings of the ASME Winter Annual Meeting.* Chicago, IL, November 16-21, 1980.

[7] Kanade, T., Khosla, P. K. and Tanaka, N.
Real-Time Control of the CMU Direct Drive Arm II Using Customized Inverse Dynamics.
In Polis, M. P. (editor), *Proceedings of the 23rd IEEE Conference on Decision and Control*, pages 1345-1352. Las Vegas, NV, December 12-14,, 1984.

[8] Khosla, P. K.
Real-Time Control and Identification of Direct-Drive Manipulators.
PhD thesis, Department of Electrical and Computer Engineering, Carnegie-Mellon University, August , 1986.

[9] Khosla, P. K. and Kanade, T.
Parameter Identification of Robot Dynamics.
In Franklin, G. F. (editor), *Proceedings of the 24-th CDC*, pages 1754-1760. Florida, December 11-13, 1985.

[10] Khosla, P. K. and Kanade, T.
Real-Time Implementation and Evaluation of Model-Based Controls on CMU DD ARM II.
In Bejczy, A. K. (editor), *1986 IEEE International Conference on Robotics and Automation*. IEEE, April 7-10, 1986.

[11] Leahy, M. B., Valavanis, K. P. and Saridis, G. N.
The Effects of Dynamics Models on Robot Control.
In *Proceedings of the 1986 IEEE Conference on Robotics and Automation*. IEEE, San Francisco, CA, April, 1986.

[12] Neuman, C. P. and Khosla, P. K.
Identification of Robot Dynamics: An Application of Recursive Estimation.
In Narendra, K. S. (editor), *Advances in Adaptive Systems Theory*. Plenum Publishing Corporation, New York, 1985.

[13] Schmitz, D., Khosla, P. K. and Kanade, T.
Development of CMU Direct-Drive Arm II.
In Hasegawa, Yukio (editor), *Proceedings of the 15-th International Symposium on Industrial Robotics*. Tokyo, Japan, September, 11-13, 1985.

[14] Slotine, J-J. E.
The Robust Control of Robot Manipulators.
International Journal of Robotics Research 4(2):81-100, Summer, 1985.

[15] Tourassis, V. D.
Dynamic Modeling and Control of Robotic Manipulators.
PhD thesis, Department of Electrical and Computer Engineering, Carnegie-Mellon University, June, 1985.